

Electronic Supplementary Information of:

Modulated excitation extended X-ray absorption fine structure spectroscopy

Gian Luca Chiarello^{1,2*}, Davide Ferri³

¹ *Università degli Studi di Milano, Dipartimento di Chimica, Via C. Golgi 19, I-23133 Milano, Italy*

² *Empa, Swiss Federal Laboratories for Materials Science and Technology, Ueberlandstrasse 129,
CH-8600 Dübendorf, Switzerland*

³ *Paul Scherrer Institut, CH-5232 Villigen PSI, Switzerland*

* Corresponding author.

Tel: +39 02 503 14281; fax: +39 02 503 14300

e-mail address: gianluca.chiarello@unimi.it

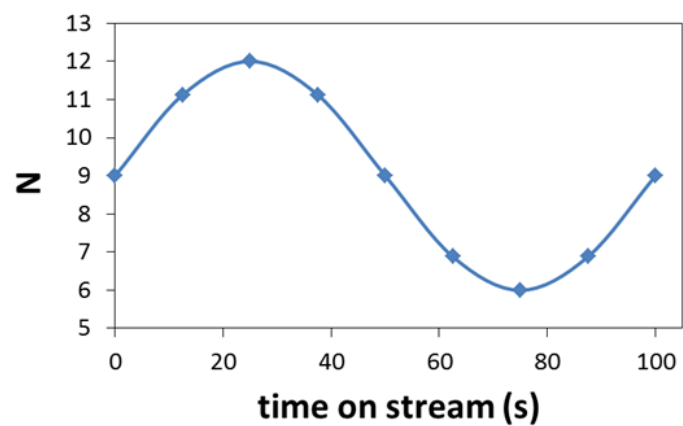


Figure S1. Simulated sinusoidal temporal variation of coordination number N (from 12 to 6) within a modulation period of 100 s.

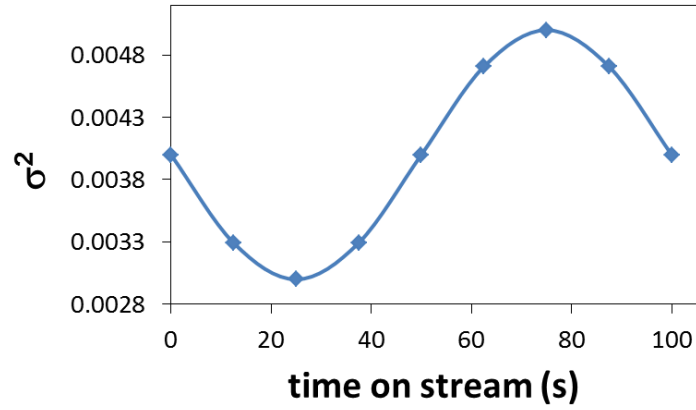


Figure S2. Simulated sinusoidal temporal variation of Debye-Waller factor σ^2 (from 0.003 \AA^2 to 0.005 \AA^2) within a period of 100 s.

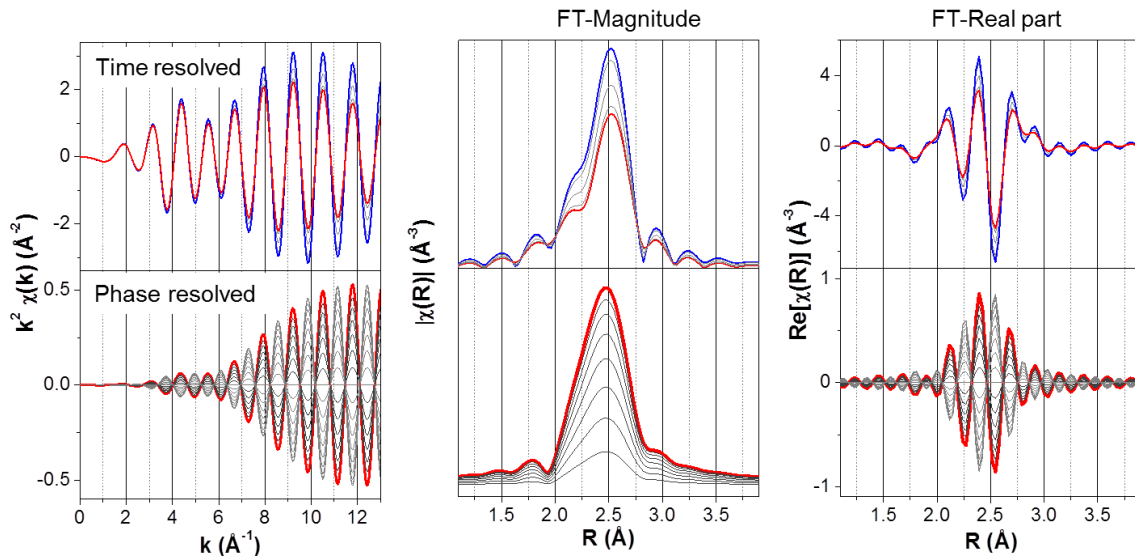


Figure S3. Effect of variation of Debye-Waller factor σ^2 (according to Fig. S2) of a single Pd-Pd first coordination shell on (left panel) the simulated k^2 -weighted $\chi(k)$ EXAFS spectra, (central panel) the FT-magnitude $|\chi(R)|$ and (right panel) the FT-real part $\text{Re}[\chi(R)]$. Top panels: simulated time-resolved spectra where σ^2 varies from 0.003 \AA^2 (blue curve) to 0.005 \AA^2 (red curve) with a phase lag $\phi = 0^\circ$ ($R = 2.758 \text{ \AA}$, $N = 12$, $\Delta E = 0 \text{ eV}$). Bottom panels: corresponding phase-resolved spectra, where the red curve corresponds to the “in-phase angle” ($\phi^{\text{PSD}} = \phi = 0^\circ$).

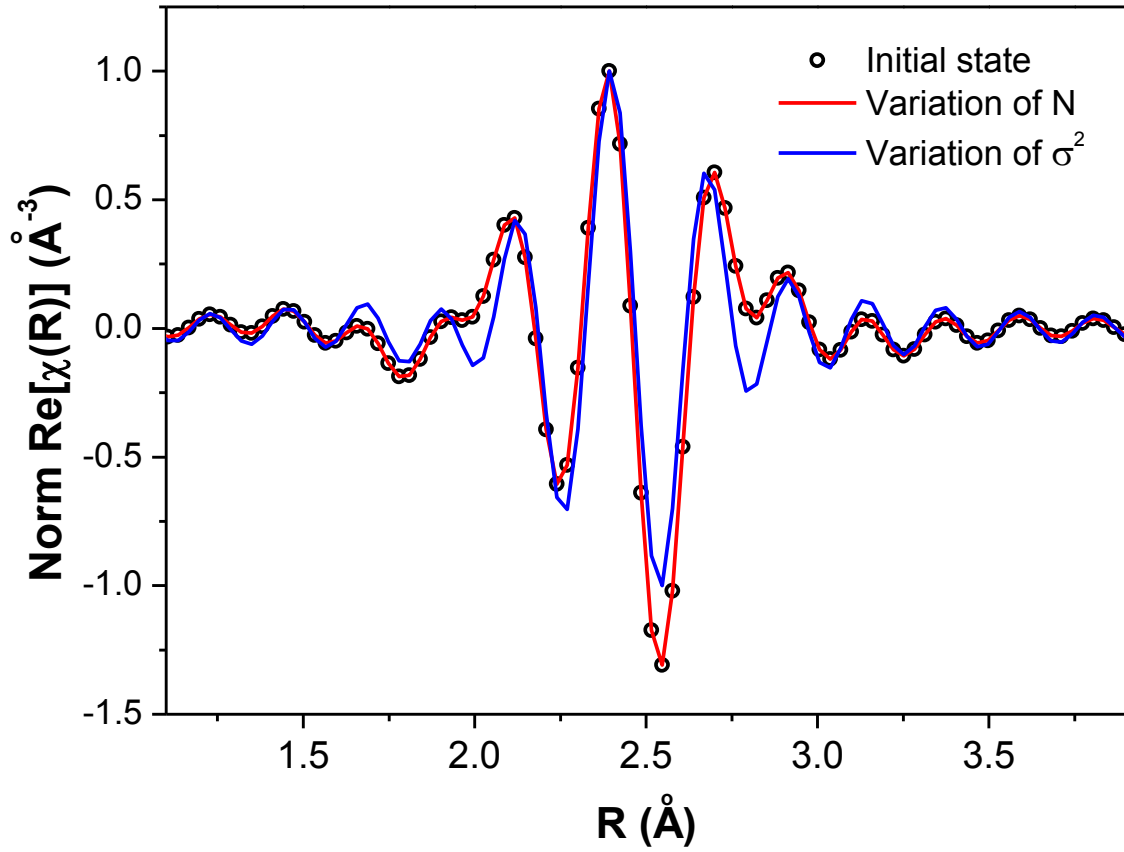


Figure S4. Effect of the variation of N (red line) or σ^2 (blue line) on the phase resolved (in-phase demodulation angle) normalized (divided by the maximum value) FT-real part with respect to that of initial state (o). Because N effects only the magnitude of $\chi(k)$ the normalized phase resolved $\text{Re}[\chi(R)]$ overlaps with that of the initial state. By contrast, because of the k -dependent effect of σ^2 on the amplitude of $\chi(k)$ a variation of σ^2 leads to a distortion of the corresponding phase resolved $\text{Re}[\chi(R)]$.

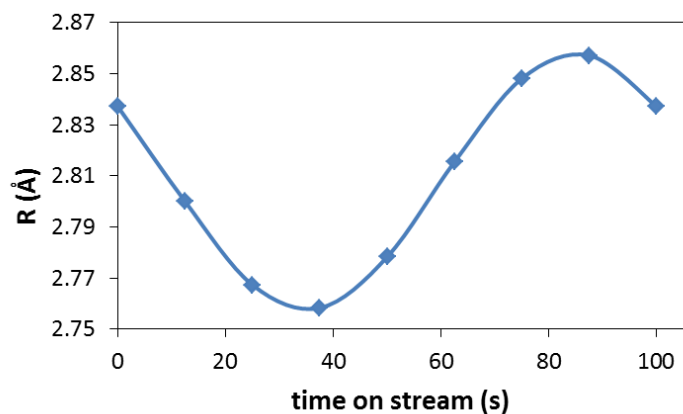


Figure S5. Simulated sinusoidal temporal variation of interatomic distance R increasing from 2.7577 Å to 2.8577 Å within a period of 100 s.

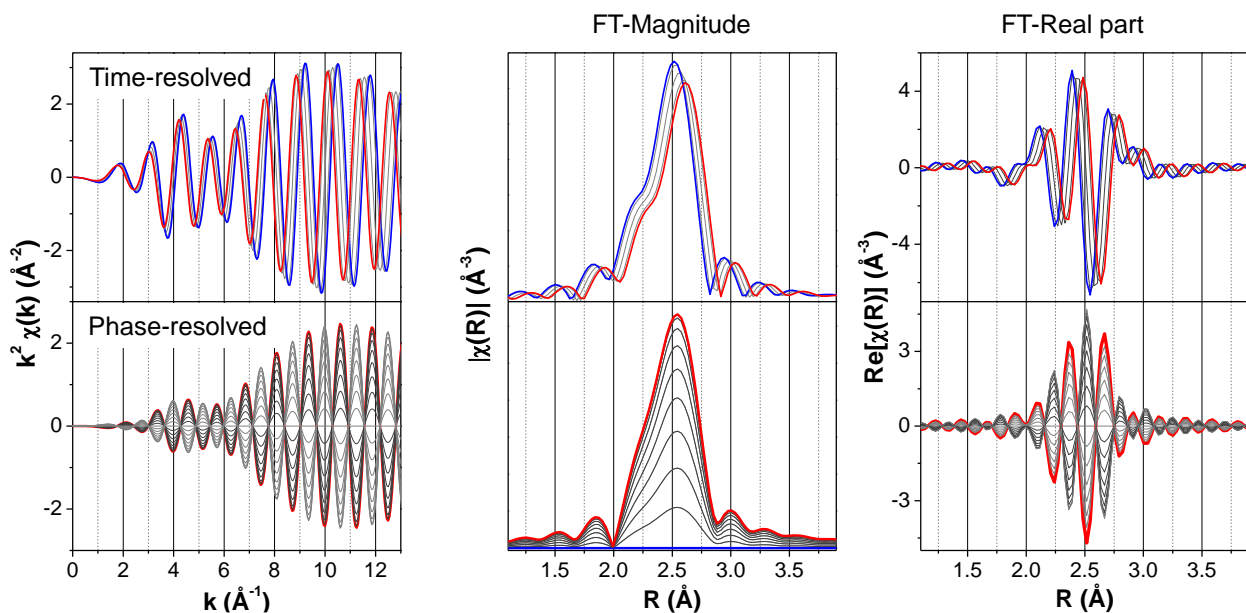


Figure S6. Effect of variation of interatomic distance R (according to Fig. S5) of a single Pd-Pd first coordination shell on (left panel) the simulated k^2 -weighted $\chi(k)$ EXAFS spectra, (central panel) the FT-magnitude $|\chi(R)|$ and (right panel) the FT-real part $\text{Re}[\chi(R)]$. Top panels: simulated time-resolved spectra where R varies from 2.7577 Å (blue curve) to 2.8577 Å (red curve) with a phase lag $\phi = 0^\circ$ ($\sigma^2 = 0.003 \text{ \AA}^2$, $N = 12$, $\Delta E^\circ = 0 \text{ eV}$). Bottom panels: corresponding phase-resolved spectra, where the red curve corresponds to the “in-phase angle” ($\phi^{\text{PSD}} = \phi = 0^\circ$).

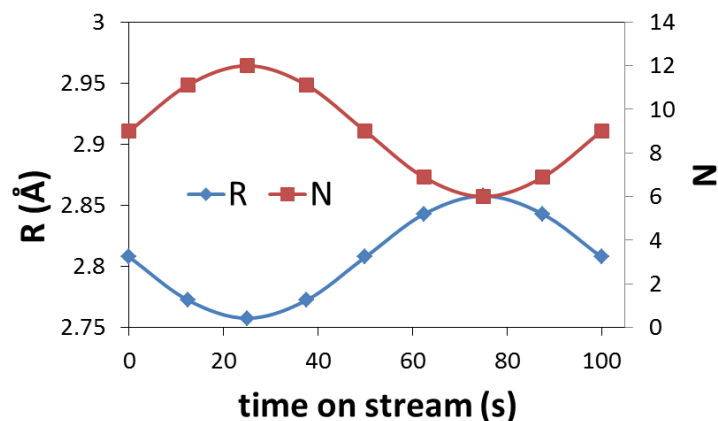


Figure S7. Simulated sinusoidal temporal variation of coordination number N (from 12 to 6) while the interatomic distance R increases from 2.7577 Å to 2.8577 Å, within a period of 100 s. Both parameters have the same phase lag ($\phi_N = \phi_R = 0^\circ$).

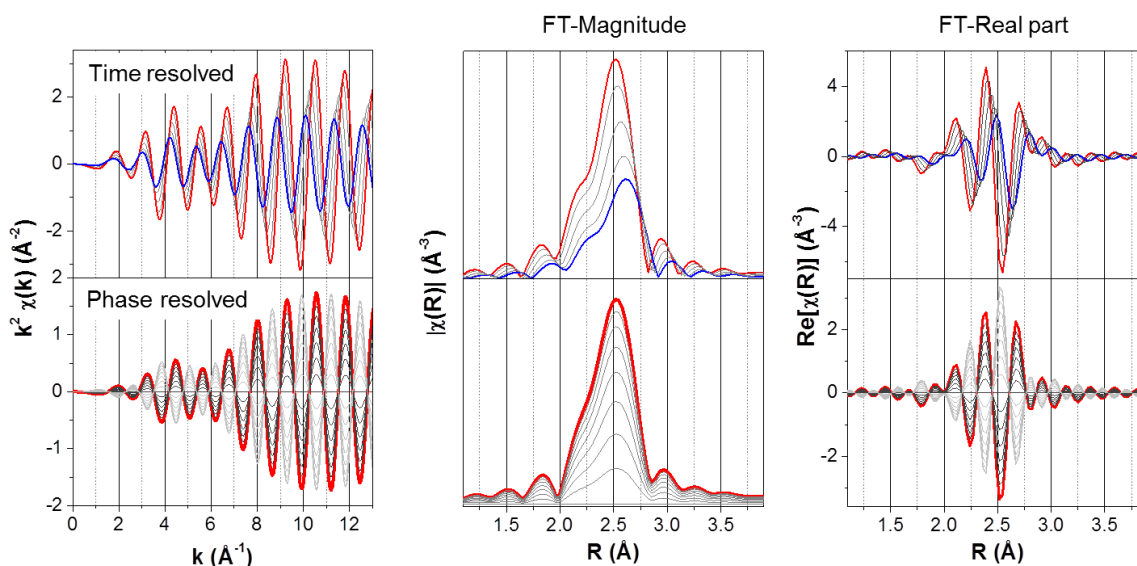


Figure S8. Effect of simultaneous variation of coordination number N and interatomic distance R (according to Fig. S7) of a single Pd-Pd first coordination shell on (left panel) the simulated k^2 -weighted $\chi(k)$ EXAFS spectra, (central panel) the FT-magnitude $|\chi(R)|$ and (right panel) the FT-real part $\text{Re}[\chi(R)]$. The upper plots show the simulated time resolved spectra where N and R vary from 12 and 2.7577 Å (red curve) to 6 and 2.8577 Å (blue curve) with a phase lag $\phi = 0^\circ$ ($\sigma^2 = 0.003 \text{ \AA}^2$ and $\Delta E^0 = 0 \text{ eV}$). The lower plots show the phase resolved spectra, where the red curve corresponds to the “in phase angle” ($\phi^{\text{PSD}} = \phi = 0^\circ$, in this case).

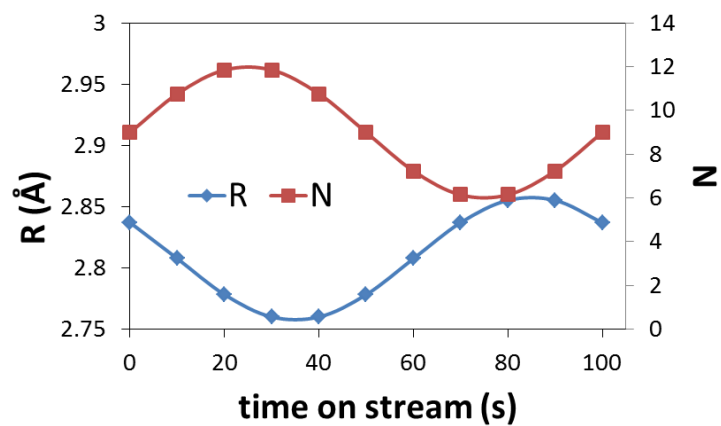


Figure S9. Simulated sinusoidal temporal variation of coordination number N (from 12 to 6) while the interatomic distance R increases from 2.7577 Å to 2.8577 Å, within a period of 100 s. The two parameters vary with different phase lag ($\phi_N = 0^\circ$, $\phi_R = 320^\circ$).

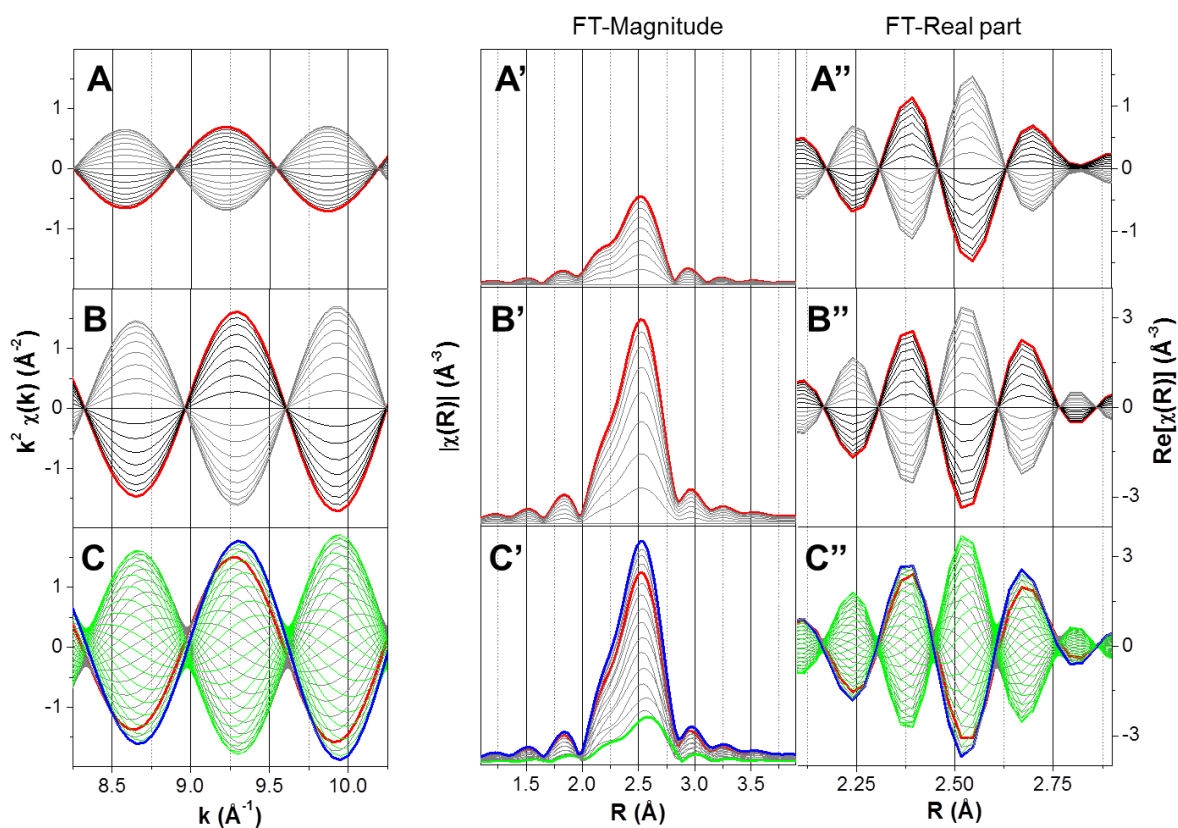


Figure S10. Effect on the simulated phase-resolved EXAFS spectra of a single Pd-Pd first coordination shell at the Pd K-edge ($0^\circ < \varphi^{\text{PSD}} < 360^\circ$) of the variation of (A) the coordination number N only; (B) coordination number N and interatomic distance R with the same phase lag, (C) coordination number N and interatomic distance R with different phase lag. Left panels: k^2 -weighted $\chi(k)$. Middle panels: FT-magnitude, $|\chi(R)|$. Right panels: FT real part, $\text{Re}[\chi(R)]$.

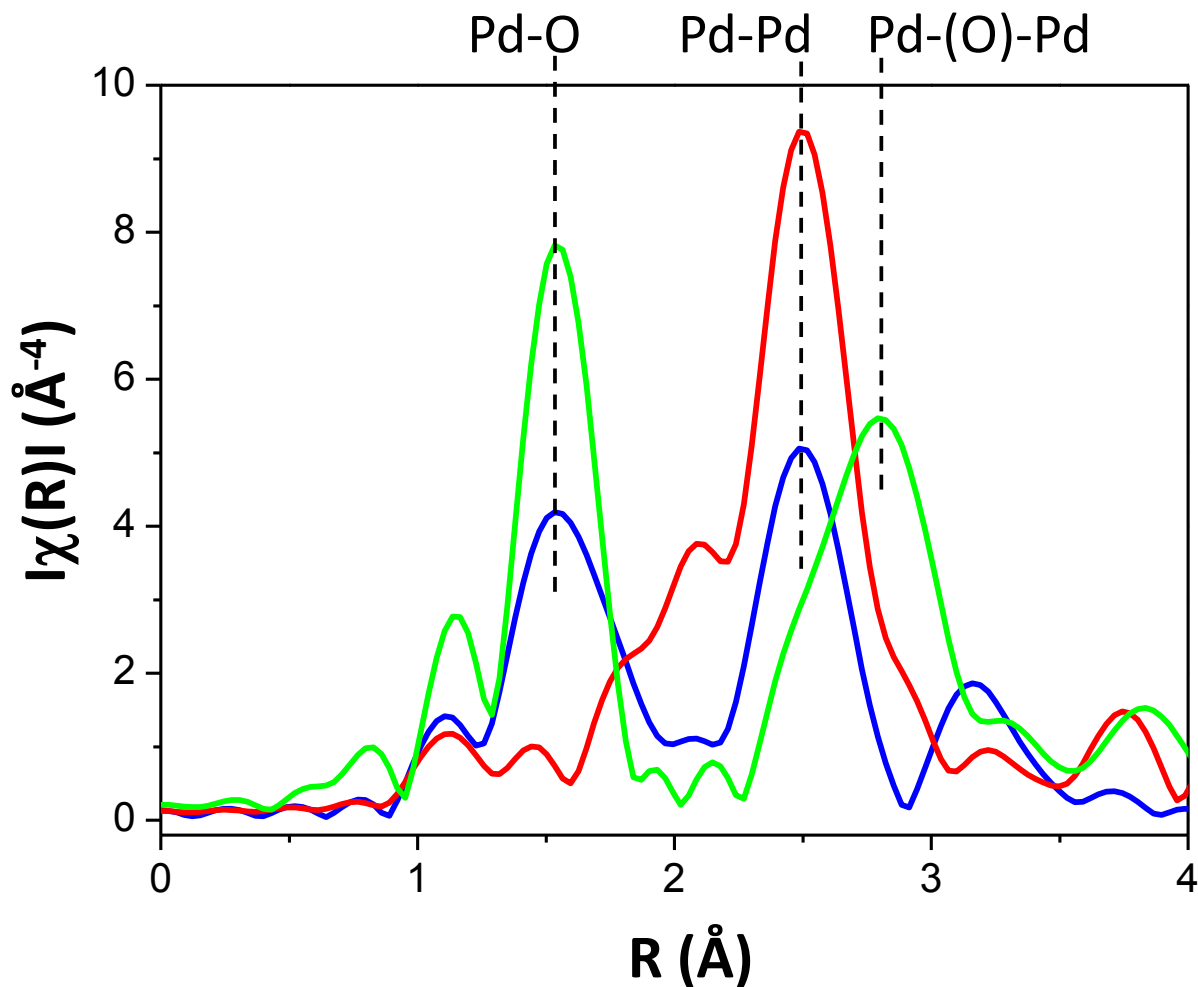


Figure S11. Comparison of the first time-resolved k^3 -weighted FT-EXAFS spectra at the Pd K-edge of 1.6 wt% Pd/Al₂O₃ recorded at the beginning of the modulation experiment at 573 K showing the structure of the catalyst after the heating pre-treatment in 1 vol% O₂/He (green curve) with the last averaged (over 28 cycles, after deleting the first 2 cycles) time-resolved k^3 -weighted FT-EXAFS recorded in 1 vol% H₂/He (red curve) and in 1 vol% O₂/He (blue curve).

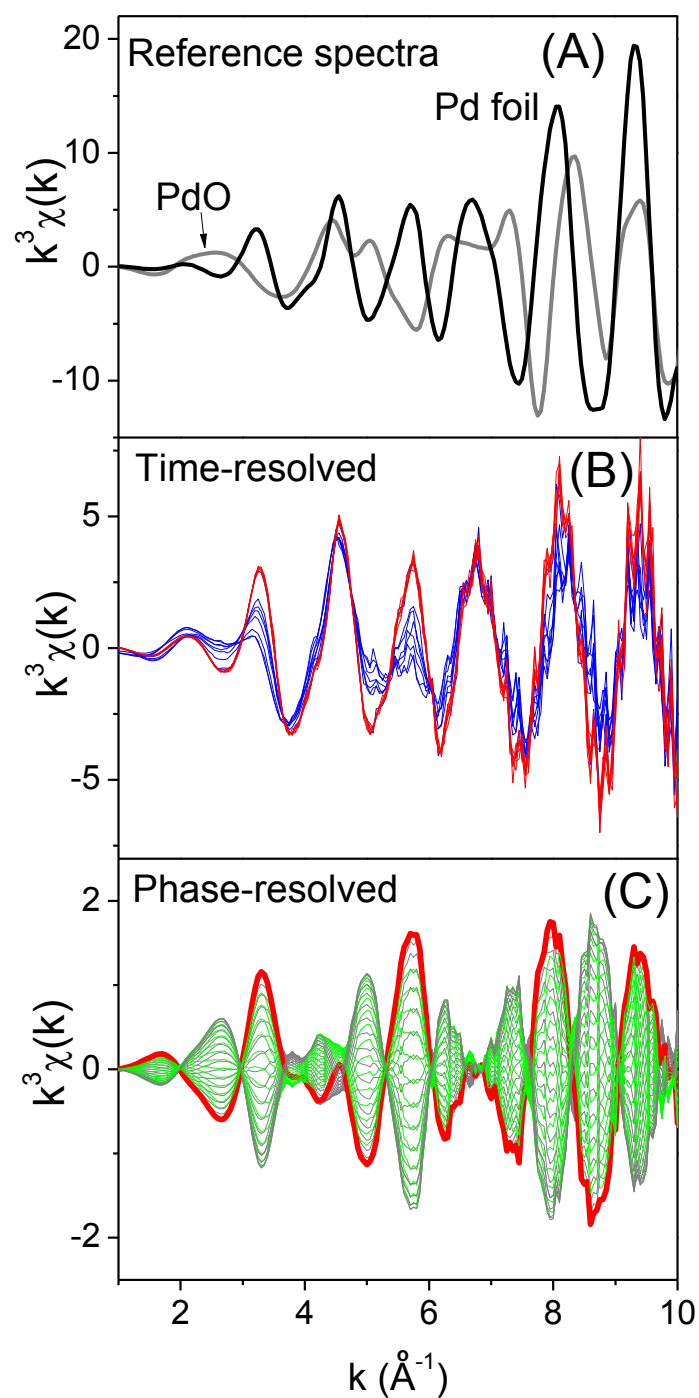


Figure S12. Experimental ME-EXAFS data at the Pd K-edge obtained on 1.6 wt% Pd/Al₂O₃ during a 1 vol% O₂/He to 1 vol% H₂/He modulation experiment at 573 K. (A) k^3 -weighted $\chi(k)$ EXAFS spectra of reference PdO and Pd foil; (B) averaged time-resolved k^3 -weighted $\chi(k)$ EXAFS spectra recorded (blue) in 1 vol% O₂/He and (red) in 1 vol% H₂/He; (C) phase-resolved k^3 -weighted $\chi(k)$ EXAFS spectra ($0^\circ < \varphi < 360^\circ$; red is $\varphi^{\text{PSD}} = \varphi_{\text{Pd-Pd}} = 160^\circ$; green curves are $170^\circ < \varphi^{\text{PSD}} < 340^\circ$, gray curves are remaining angles).